

Article

Not peer-reviewed version

# SIK2 Controls the Homeostatic Character of POMC Secretome Acutely in Response to Pharmacological ER Stress Induction

[Mehmet Soner Türküner](#), [Ayşe Yazıcı](#), [Ferruh Özcan](#)\*

Posted Date: 8 August 2024

doi: 10.20944/preprints202408.0611.v1

Keywords: SIK2; POMC; inflammation; neuronal secretome; ER stress; hypothalamic obesity



Preprints.org is a free multidiscipline platform providing preprint service that is dedicated to making early versions of research outputs permanently available and citable. Preprints posted at Preprints.org appear in Web of Science, Crossref, Google Scholar, Scilit, Europe PMC.

Copyright: This is an open access article distributed under the Creative Commons Attribution License which permits unrestricted use, distribution, and reproduction in any medium, provided the original work is properly cited.

Article

# SIK2 Controls the Homeostatic Character of POMC Secretome Acutely in Response to Pharmacological ER Stress Induction

Mehmet Soner Türküner <sup>1,2</sup>, Ayşe Yazıcı <sup>1,2</sup> and Ferruh Özcan <sup>1,2,\*</sup>

<sup>1</sup> Department of Molecular Biology and Genetics, Graduate School of Natural and Applied Sciences, Gebze Technical University (GTU), Gebze, Kocaeli, 41400, Turkey

<sup>2</sup> Cellular Proteomics Laboratory, Gebze Technical University - Central Research Laboratory, Application and Research Center Laboratory (GTU-MAR)

\* Correspondence: ferruh.ozcan@gtu.edu.tr; Tel.: +90 262 605 25 08/49

**Abstract:** The neuronal etiology of obesity is centered around diet-induced inflammatory state in the arcuate nucleus of the hypothalamus which impairs the functionality of pro-opiomelanocortin neurons (POMCs) responsible for whole-body energy homeostasis and feeding behavior. Intriguingly, systemic salt inducible kinase 2 (SIK2) knockout mouse demonstrated reduced food intake and energy expenditure along with modestly dysregulated metabolic parameters suggesting a causal link between the absence of SIK2 activity in POMCs and the observed phenotype. To test this hypothesis, we conducted a comparative secretomics study from POMC neurons following pharmacologically induced endoplasmic reticulum (ER) stress induction, a hallmark of metabolic inflammation and POMC dysregulation in diet induced obese (DIO) mice. Our data provide significant *in vitro* evidence for the POMC specific SIK2 activity in controlling the energy metabolism and feeding in DIO mice by regulating the nature of related POMC secretome. Our data also suggests that under physiological stress conditions SIK2 may act as a *gatekeeper* for the secreted inflammatory factors and signaling molecules critical for cellular survival and energy homeostasis. On the other hand, in the absence of SIK2 gate opens leading to surge of inflammatory cytokines and apoptotic cues concomitant with the dysregulation of POMC neurons.

**Keywords:** SIK2; POMC; inflammation; neuronal secretome; ER stress; hypothalamic obesity

## Introduction

A paradigm shift in the etiology of obesity occurred when it became clear that low-grade metabolic inflammation was detected in several brain regions, particularly in the arcuate nucleus (ARC) of the hypothalamus even before the onset of obesity. The ARC of the hypothalamus is a key regulatory center for the whole-body energy homeostasis and feeding behavior and transmits signals between the periphery and the central nervous system (CNS) [1]. The two functionally opposing neuronal subpopulations consisting of pro-opiomelanocortin (POMC) and neuropeptide Y/agouti-related protein (NPY/AgRP) neurons in the ARC integrate peripheral and central inputs and communicate with their downstream effectors through various secreted proteins for the maintenance of organismal energy balance [1,2]. In the low-energy state, some gut-derived hormones, such as ghrelin, activate orexigenic NPY/AgRP neurons, which stimulate food intake and suppress energy expenditure [3]. In contrast, in the excess energy state, nutrient-related hormones, such as leptin and insulin, activate anorexigenic POMC neurons, which enhance energy expenditure while decreasing food intake [4,5]. POMC, which is expressed as a precursor, undergoes a series of posttranslational cleavages, resulting in the secretion of biologically active neuropeptides (such as  $\alpha/\beta$ -melanocyte-stimulating hormone ( $\alpha/\beta$ -MSH), adrenocorticotrophic hormone (ACTH), and  $\beta$ -endorphin) [6] in addition to fast neurotransmitters such as  $\gamma$ -aminobutyric acid (GABA) [7]. These neuropeptides play important roles in various physiological processes, including microglial inflammation [8], pigmentation [9], stress response, and energy balance [10,11]. POMC neurons project specifically to

the paraventricular (PVH) and dorsomedial (DMH) nuclei of the hypothalamus, the lateral hypothalamic area (LHA) [7,12] and the medial amygdala [13]. POMC neuron-derived neuropeptides bind to their cognate receptor, melanocortin 4 receptor (MC4R), on these neuronal subpopulations, thereby inducing signaling cascades to maintain energy homeostasis.

Salt inducible kinase 2 (SIK2), an AMP-activated protein kinase (AMPK) family member, is highly expressed in adipose tissue and the liver [14] and plays a pivotal role in glucose and lipid metabolism [15]. Previous studies have emphasized the possible modulatory functions of SIK2 in neuronal survival [16] and proteinopathy-related diseases [17]. SIK2 reduces the nuclear translocation of target of rapamycin (TOR) complex-2 (TORC2) and corticotropin-releasing hormone (CRH) transcription in the hypothalamic neurons of rats in a stress-dependent manner [18]. SIK2 contributes to insulin secretion in pancreatic beta cells by promoting calcium influx via Voltage-dependent calcium channels [19]. SIK2 and SIK3 were implicated in macrophage polarization and secretion of inflammatory cytokines in monocytes and mast cells, respectively [20,21]. SIK2-mediated phosphorylation of valine-containing protein (VCP)/p97 upregulates endoplasmic reticulum-associated degradation (ERAD)-mediated degradation and autophagy [22]. Autophagosomes are known to participate in the secretion of leaderless proteins, although the molecular mechanisms related to vesicular diversification between autophagosomes and the secretion of vesicles have yet to be elucidated.

The total secretome, a collection of proteins secreted or shed by cells, plays a central role in many biological processes and shapes the microenvironment of cells [23]. The content of the neuronal secretome plays a crucial role in neuroprotection, neurodegeneration, and signal transmission in health and disease conditions [24], such as Parkinson's disease [25] and amyotrophic lateral sclerosis (ALS) [26], underscoring its therapeutic potential. Hypothalamic inflammation is characterized by an abrupt surge of chemokines, including fractalkine (CXCL3), monocyte chemoattractant protein-1 (MCP-1), tumor necrosis factor- $\alpha$  (TNF- $\alpha$ ), interleukin-6 (IL-6), and a few others, which act on POMC neurons by altering their secreted neuropeptides and neurotransmitters, which further aggravates the inflammatory state culminating in POMC-mediated dysregulation of food intake and energy expenditure [27,28]. Although controversial data exist for the cellular origin and significance of hypothalamic inflammation in obesity development, future design centrally acting anti-obesity drugs will most likely target the specific links between the neurons of the feeding circuitry via their secreted neuropeptides and/or neurotransmitters.

Earlier reports have demonstrated that low-grade metabolic inflammation in the hypothalamic arcuate nucleus of obese animal models can alter the expression of anorectic POMC and thereby its derivative neuropeptides, altering the feeding behavior and energy metabolism of the organism [29]. *In vivo* studies with obese animal models (DIO) have demonstrated a correlation between hypothalamic inflammation and ER stress and the lipid content of a high-fat diet (HFD) [30]. In our *in vitro* model system we primarily aimed at probing the effects of chemically induced ER stress and its downstream effector kinase SIK2 on POMC secretome to avoid compounding effects associated with the use of physiologically relevant palmitate [31]. In this study, our strategy was to elucidate SIK2-mediated changes in the ER-stressed POMC secretome that may contribute to disease etiopathogenesis. In the end, these neuropeptides may provide therapeutically invaluable targets for the treatment of obesity and associated diseases.

## 2. Materials and Methods

### 2.1. Cell Culture and Chemical Treatments

The mouse hypothalamic proopiomelanocortin cell line *mHypoA-POMC/GFP-2* (POMCs) was initially derived from the arcuate nucleus of the mouse, expressing EGFP transgene was driven by the POMC promoter through the use of fluorescence-activated cell sorting (FACS). It has been previously demonstrated that these cells secrete  $\alpha$ -MSH and, consistent with their origin, respond to anorectic hormones such as insulin and leptin as well as the ER stressor palmitate. Consequently, it has been reported that these cells can be used as accurate *in vitro* models for the discovery,

development, and validation of novel therapeutics targeting central nervous system-based diseases and disorders, including obesity, stress, and metabolic disorders [32,33].

POMCs and human embryonic kidney (HEK) 293FT cells were purchased from CEDARLANE (Canada) and Invitrogen (USA), respectively. The cells were maintained in complete high-glucose DMEM (Gibco, Canada) supplemented with 10% fetal bovine serum (Gibco) and 1% penicillin/streptomycin (Gibco) at 37°C and 5% CO<sub>2</sub>. The cells were cultured to 70-80% confluence and passaged as suggested by the vendor.

The thapsigargin (THA) (Sigma Aldrich, USA), which is a chemical agent causing calcium depletion in the ER by inhibiting sarco/endoplasmic reticulum Ca<sup>2+</sup> transport ATPase (SERCA), was used as an ER stress inducer. It was dissolved in DMSO (Sigma Aldrich), which was used as a control group in the experiments. ER stress induction with THA (100 nM) [34] was verified by an increase in the level of the luminal chaperone glucose-regulated protein 78 (GRP78/BiP) by immunoblotting (CST, USA).

## 2.2. Cell Viability Assays

To investigate the cytotoxicity of THA on POMCs, 5,000 cells were seeded in each well of a 96-well plate. After 24 h, the cells were treated with 100 nM THA and vehicle (DMSO) for the indicated durations (6, 12, and 24 h). In the last 4 hours of treatment, 10 µl of the cell proliferation reagent WST-1 (Roche, Germany) was added to the wells. The cells were incubated for 4 hours at 37°C with 5% CO<sub>2</sub>. Spectrophotometric measurements were performed at 450 nm (with 600 nm as a reference wavelength) by using a Varioskan Flash Reader (Thermo Scientific, USA).

To examine the viability of POMCs under THA and serum-free conditions, 25,000 cells were seeded in a 24-well plate. After 24 h, under serum-depleted conditions, the cells were washed 3 times with 1× PBS (LONZA, Switzerland) and then treated with 100 nM THA and vehicle DMSO in 0% serum-containing media for 6 and 12 h. For serum-containing conditions, treatment was performed directly in the supplemented media. The percentage of the dead cells were quantified by counting viable cells with trypan blue under a DMi1 light microscope (Leica, Germany).

## 2.3. Preparation of Molecular Cloning and Manipulation Cell Lines

### 2.3.1. Transient Overexpression System

Wild-type (WT) SIK2 was subcloned and inserted into the pCMV-3Tag-6 expression vector (#240200 Agilent, USA) from the pDream\_mSIK2 WT plasmid containing the synthetic mouse SIK2 gene (Genescript, USA). For this cloning, a proper primer pair was designed by using the cloud-based platform Benchling (San Francisco) and Oligo Analyzer tool (IDT, USA), and then the primer pair was synthesized by Macrogen (Seoul, South Korea) (**Table 1**). The gene was inserted from donor plasmids by using high-fidelity PrimeStar HS DNA Polymerase (Takara, USA). The produced insert and targeted plasmid were cut by fast digest restriction enzymes (Thermo Scientific, USA) and extracted from a 1% agarose gel by using an MN Gel Extraction or PCR Clean-Up Kit (Macherey-Nagel, Germany). Ligation of the prepared insert and plasmid via T4 DNA Ligase (NEB, USA) and transformation of the ligation products into competent DH5α cells were performed via the conventional transformation method (Addgene, USA). After obtaining colonies, colony PCRs were performed with the designed primer pair and Taq DNA Polymerase (ABM, Canada) to identify possible positive colonies. To further confirm the presence of the insert within the recombinants, plasmids were isolated from the detected colonies by a DNA-spin Plasmid DNA Purification Kit (iNtRON Biotechnology, South Korea) and were reconstituted with the same restriction enzymes that were used during the cloning step to observe the inserts. At least three of the confirmed colonies were selected and sequenced (Macrogen) to perform the final control. Finally, the pCMV-3Tag6-mSIK2\_WT plasmid was isolated using the MN NucleoBond Xtra Midi Kit (MN, Germany) to obtain transfection-grade plasmids.

To generate flag-tagged SIK2 WT overexpressing and control POMC cells, the pCMV-3Tag6-mSIK2\_WT plasmid and empty pCMV-3tag6 plasmid was transfected into POMCs, respectively,

using polyethyleneimine (PEI-MAX) (Polysciences, UK). To increase the transfection efficiency, a series of optimizations of salt ions and related parameters that affect PEI-DNA particles were performed based on a previous report [35]. A total of 800,000 cells were seeded in 10 cm cell culture dishes. After 24 h, 15 µg of plasmid DNA and PEI were incubated in 1× Tris/EDTA buffer containing 150 mM NaCl (pH 8.0) at a ratio of 1:3 (w:w) for 10 min, after which the PEI: DNA particles were distributed throughout the cells. After 6 h, the media of the cells were replaced with fresh complete DMEM. Transiently transfected POMC cells were used for experiments at 48-72 h post-transfection.

### 2.3.2. Lentivirus-Based Stable shRNA System

For RNA interference-based SIK2 knockdown (KD), three different shRNA oligos that target endogenous SIK2 mRNA, which is complementary to the indicated exon positions, were designed by using the siRNA selection tool WI siRNA Selection Program (MIT, USA) based on the design rules of the Broad Institute [36] (**Table 1**). Synthesized oligos from Macrogen (South Korea) were cloned and inserted into the lentiviral pLKO.1 TRC cloning vector (#10878 Addgene, USA) was used according to the suggested protocols [37]. At least three confirmed clone colonies were selected and sent to Macrogen for sequencing. The confirmed plasmids were isolated using an MN NucleoBond Xtra Midi Kit (MN, Germany) to obtain transfection-grade plasmids.

To produce lentiviral particles, one day before transfection, 293FT cells were seeded in 6 cm cell culture dishes at 80-90% confluence on the day of transfection. Lentiviral packaging was performed by transferring 2nd Generation Packaging System from Addgene; 3 µg of psPAX2 (#12260), 2 µg of pCMV-VSVG (#84549), and 4 µg of cloned pLKO.1-TRC lentiviral expression vectors into 293FT cells by PEI-based transfection (as described previously). Following a 48-hour and 72-hour period of transfection, the media containing viral particles were harvested via centrifugation (1500 rpm for 5 minutes) and then filtered (0.45-µm filter unit attached to a syringe) from the 293FT cells. The viral particles were aliquoted for single use at -80°C. To generate stable SIK2-KD and scrambled POMC cell lines, 100,000 cells were seeded in a 6-well plate. After 24 h, lentiviral transduction was performed using 8 µg/ml of the cationic polymer hexadimethrine bromide (polybrene) (Sigma Aldrich, USA). Stable cells were obtained following selection with 5 µg/ml puromycin (Santa Cruz Biotech, USA) for 14 days. Stable POMCs were tested for their knockdown efficiency. Each shRNA suppressed SIK2 expression by approximately 70-80% (**Figure 1A**). SIK2-KD POMCs containing Exon2 were selected for further experiments and stable scramble-POMCs were used for the RNAi control group.

**Table 1.** Molecular cloning primers for the overexpression and shRNA systems.

Primer Name	Oligo Set
<i>2F_KpnI (Tm: 61)</i>	AAAAAGGTACCATGGTCATGGCGGATG
<i>2R_KpnI (Tm: 64)</i>	AAAAGGTACCCTAGGTCTCCCGGGCTAAG
<i>mSIK2_Exon2_ shRNA_F</i>	CCGGAATCTACCGAGAAGTACAGATCTCGAGATCTGTACTTCTCGG TAGATTTTTTTG
<i>mSIK2_Exon2_ ShRNA_R</i>	AATTCAAAAAAATCTACCGAGAAGTACAGATCTCGAGATCTGTAC TTCTCGGTAGATT
<i>mSIK2_Exon4_ shRNA_F</i>	CCGGAATTCTGTCTGCTGTTGATTACTCGAGTAATCAACAGCAGAC AGAATTTTTTTG
<i>mSIK2_Exon4_ ShRNA_R</i>	AATTCAAAAAAATCTGTCTGCTGTTGATTACTCGAGTAATCAACA GCAGACAGAATT
<i>mSIK2_Exon5_ shRNA_F</i>	CCGGAAGGACCACAGCTGGATATATCTCGAGATATATCCAGCTGTG GTCCTTTTTTTTG
<i>mSIK2_Exon5_ shRNA_R</i>	AATTCAAAAAAAGGACCACAGCTGGATATATCTCGAGATATATCC AGCTGTGGTCCTT
<i>Scrambled_ shRNA_F</i>	CCGGCCTAAGGTTAAGTCGCCCTCGCTCGAGCGAGGGCGACTTAA CCTTAGGTTTTTG

<i>Scrambled_</i>	AATTCAAAAACCTAAGGTTAAGTCGCCCTCGCTCGAGCGAGGGCG
<i>shRNA_R</i>	ACTTAACCTTAGG

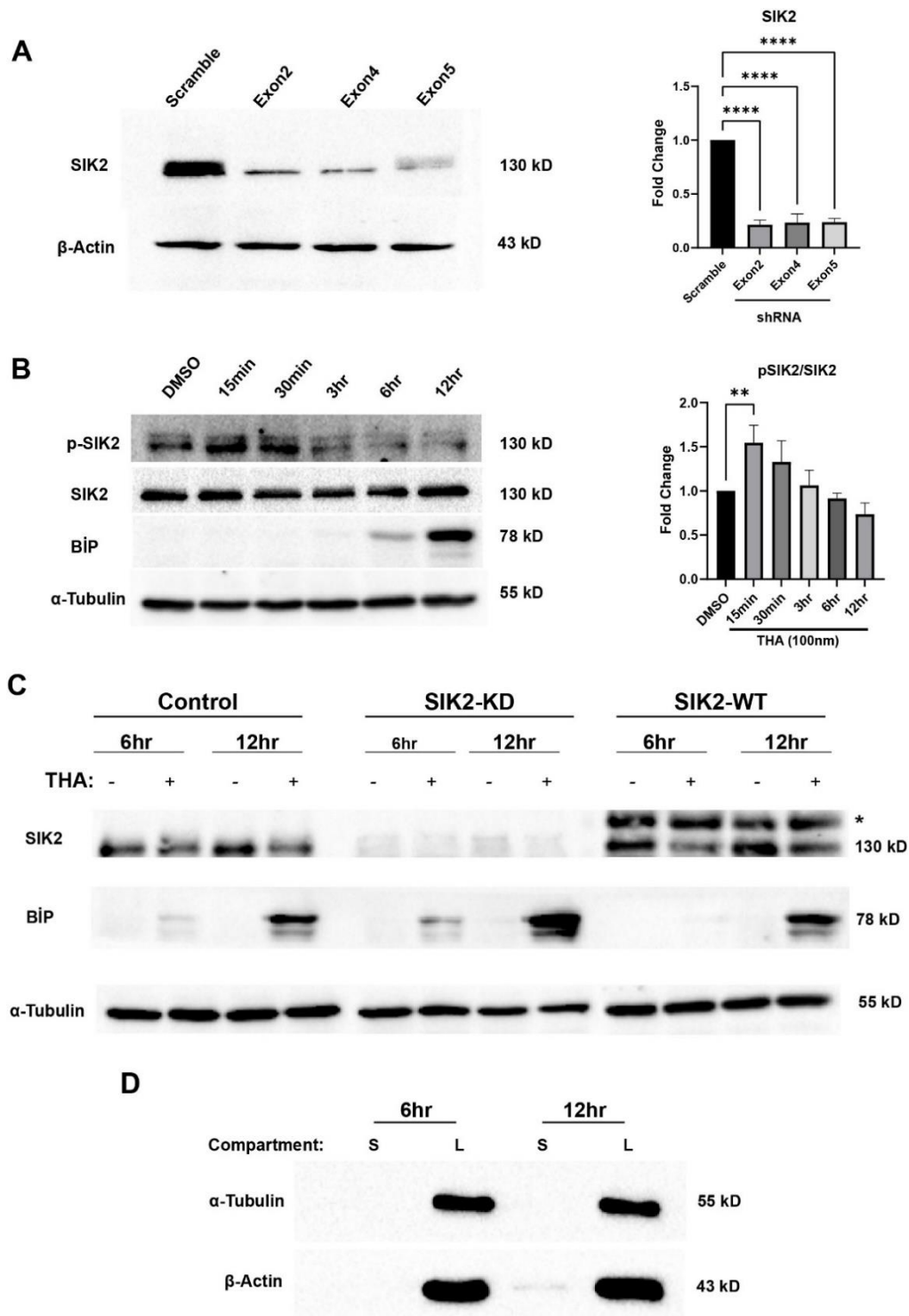


**Figure 1. Confirmation of stable POMCs and secretomes.** A) Stable SIK2 KD POMC cell candidates carrying three different shRNAs were analyzed for SIK2 protein levels. The bar chart illustrates the expression level of SIK2 ( $n=3$ ). B) SIK2 activation was confirmed via the expression of phospho-SIK2 (Thr175) and SIK2 under 100nm THA as indicated time points. The bar chart illustrates the ratio of phospho-SIK2 to the total SIK2 ( $n=3$ ). C) SIK2 manipulations were confirmed via immunoblotting on SIK2-knockdown (SIK2 KD), SIK2-overexpressing (SIK2 WT), and control POMC cells were treated with 100nm THA for 6 and 12 hours. ER stress was also confirmed by BiP expression ( $n=3$ ). \*Shifted band indicates 3xflag-tagged SIK2. D) The purified secretomes at the indicated time points were

evaluated for cytoplasmic contamination using antibodies specific for  $\alpha$ -tubulin and  $\beta$ -actin. The secretomes (S) were compared to the cellular lysates (L) ( $n=3$ ). Error bars on densitometric graphs are means  $\pm$  standard deviation (SD), for A: \*\*\*\* $P < 0.0001$ , for B: \*\* $P < 0.01$ .

#### 2.4. Conditioned Media (CM) Isolation

To obtain a pure secretome sample, our protocol was optimized according to previous reports [38]. A total of 800,000 POMCs were seeded in 10 cm cell culture dishes. After 24 h, the cells were washed 3 times with 1x PBS (LONZA, Switzerland) and then treated with 100 nM THA and vehicle DMSO in 5 ml of 0% serum-containing DMEM for 6 and 12 h. The CMs collected from three 10 cm cell culture dishes per condition were pooled. Fifteen milliliters of medium from each condition was centrifuged at  $500 \times g$  for 5 minutes and then at  $2,000 \times g$  for 10 minutes at  $4^{\circ}\text{C}$ , and the resulting supernatant was passed through a  $0.22 \mu\text{m}$  PES filter to remove cellular debris and apoptotic bodies. The secretome samples were centrifuged at  $10,000 \times g$  for 30 minutes at  $4^{\circ}\text{C}$  to remove microvesicles and then centrifuged at  $100,000 \times g$  for 1 hour at  $4^{\circ}\text{C}$  to remove exosome vesicles. After all these serial centrifugation processes, the resulting pure secretome samples were concentrated to approximately 200-500  $\mu\text{l}$  and buffer-exchanged into 50 mM Tris, pH 8.0, using an Amicon® Ultra Centrifugal Filter with a 3 kDa MWCO (Merck, Germany). The total protein concentration was determined using a Qubit 3.0 with a Qubit Protein Assay Kit (Thermo Scientific, USA).

#### 2.5. Immunoblotting and One-Dimensional Gel Electrophoresis (1DE) Analysis

The total protein for each condition was isolated in lysis buffer (150 mM NaCl, 50 mM Tris-Cl (pH 7.4), 2 mM EDTA, 1% NP-40, 0.5% sodium deoxycholate, 5 mM NaF, 1 mM sodium orthovanadate ( $\text{Na}_3\text{VO}_4$ ), 1 mM PMSF, 5 mM aprotinin, and 1  $\mu\text{g/ml}$  leupeptin) (Applichem, Germany) by centrifugation at  $18,000 \times g$  for 15 minutes at  $4^{\circ}\text{C}$ . The total protein concentration was quantified with a Pierce BCA Protein Assay Kit (Thermo Scientific, USA). The samples were loaded equally on 5% and 10% SDS-PAGE gels and run at 80 volts. Proteins in 5% gels were transferred to PVDF membranes (Thermo Scientific) by Transblot Turbo according to the manufacturer's instructions (Bio-Rad, USA), while those in 10% gels were subjected to SybroRuby Gel Stain (Invitrogen, USA) for total protein staining according to the manufacturer's instructions. The membranes were blocked in 5% skim milk in TBS containing 0.1% Tween-20 for 1 h at room temperature and immunoblotted with the following primary antibodies: anti-SIK2 (1:1000; Cell Signaling; #6919), anti-p-SIK2 (1:1000; Invitrogen; #PA5-64607), anti-BiP (1:1000; Cell Signaling; #3177), anti- $\alpha$ -Tubulin (1:1000; Cell Signaling; #3873), and anti- $\beta$ -Actin (1:1000; Cell Signaling; #4970) overnight at  $4^{\circ}\text{C}$  and with the following secondary antibodies: anti-mouse IgG-HRP (1:3000, Santa Cruz, #sc-2005) and anti-rabbit IgG-HRP (1:3000, Santa Cruz, #sc-2357) for 2 h at room temperature. Immunoblots and gel staining were visualized with ChemiDoc XRS+ (Bio-Rad). Chemiluminescence-derived bands were detected by WesternBright ECL HRP substrate (Advansta, USA) and quantified using ImageJ software as previously reported [39].

#### 2.6. Secretome Analysis

##### 2.6.1. Sample Preparation

Five micrograms of each sample was dissolved in 50 mM Tris-HCL, pH 8.0 (Invitrogen, USA), containing 6 M urea (Invitrogen) for full denaturation. In a thermoshaker (400-500 rpm), the proteins were reduced with 500 mM tris (2-carboxyethyl) phosphine (TCEP) (Thermo Fisher, USA) (20 mM final concentration) for 1 h at  $60^{\circ}\text{C}$ , followed by alkylation using 1 M iodoacetamide (IAA) (Thermo Fisher) (40 mM final concentration) for 30 min at room temperature. After dilution (urea  $< 1$  M) with 50 mM Tris-HCL (pH 8.0), the proteins were digested with Pierce trypsin protease (Thermo Scientific) (1:20, w:w) overnight at  $37^{\circ}\text{C}$  in a thermoshaker. To stop the digestion, formic acid (1-2% final concentration) was added to each sample. The peptides were concentrated and desalted by a Pierce C18 tip (Thermo Scientific) and speed-vac.

## 2.6.2. Mass Spectrometry

The desalted and concentrated peptides were loaded onto a reverse-phase column on a nanoflow ultrahigh-performance liquid chromatography (nano-UHPLC) instrument (Ultimate 3000 RSLCnano, Thermo Fisher Scientific, USA) coupled online to an LTQ Orbitrap ELITE mass spectrometer with a nanoelectrospray ion (ESI) source (Thermo Fisher Scientific). The peptides were mixed to 200 ng/ $\mu$ l with a sampler buffer containing 5% acetonitrile and 0.1% formic acid and were introduced into the liquid chromatograph with a 2  $\mu$ l injection volume. Mobile phase A was 0.1% (v/v) formic acid, and mobile phase B was 0.1% (v/v) formic acid in 80% acetonitrile (Fisher Scientific). Peptide gradient separation was performed on a C18 column (Acclaim PepMap, RSLC 75  $\mu$ m  $\times$  250 mm) (Thermo Scientific). Peptide separation was conducted using the following gradients: 4% phase B over 5 min, 4–55% phase B over 85 min, 55% phase B over 10 min, and 55–95% phase B over 10 min, with a final elution of 95% B for 5 min at a flow rate of 300 nL/min. Each sample was analyzed by LC–MS/MS as three fractions. The data were acquired using the data-dependent acquisition (DDA) method in positive ion mode. MS1/MS2 scans were performed in *Orbitrap* and *ion trap* analyzers, respectively, with 350–1800 m/z scan ranges at 60,000 resolution. All MS<sup>n</sup> spectra were acquired using collision-induced dissociation (CID) with 35% normalized collision energy, 0.25 activation Q, a 10 ms activation time, and a 1 m/z isolation width. The data were acquired using Xcalibur 4.0 software (Thermo Scientific). The raw MS data were analyzed using Proteome Discoverer 2.3 software (PD) (Thermo Scientific).

## 2.7. Bioinformatic and Statistical Analysis

The results of the LS-MS/MS analysis for all samples are based on independent biological triplicates and three technical fractions for each experimental condition. MS/MS spectra were searched and identified against the mouse total protein database, secretome database (“Secreted” from the cellular component of Gene Ontology), and sheddome database (“Transmembrane” and “GPI anchored”) from UniProt by using Sequest HT and msAmanda 2.0 search engines. The tolerances of the precursor and fragment ions were 10 ppm and 0.5 Da, respectively. Oxidation (M), N-terminal acetylation, and carbamidomethylation were selected as the dynamic and static modifications, respectively. Peptide sequence mass (PSM) validations were performed by “Percolator” with a false discovery rate (FDR) and q value < 0.05. To investigate low-abundance proteins, spectral clustering search nodes [40] were identified with the MS Amanda 2.0 [41] engine as suggested by the developers. The spectrum clustering algorithm enhances the detectability of low-abundance proteins while simultaneously elevating the precision of the derived quantitative data, without concomitantly increasing the noise of the datasets. Additionally, msAmanda algorithm confidently provides more accurate spectra at the same FDR than Sequest on examined high-mass accuracy data sets. The combination of these nodes enabled the analysis of proteins that are low-abundant (FDR above 0.05, FDR class denotes low) but can demonstrate a notable fold change through label-free quantification (LFQ). LFQ was employed for the differential protein analysis using the Minora detection and precursor ion quantifier nodes of PD. The statistical significance of peptide abundances between groups was determined by one-way ANOVA, with a p-value of  $\leq 0.05$ . Proteins with a fold change  $\geq 2$  were considered significant. The scrambled POMC secretome was selected as the control since no significant difference was observed when it was compared to the empty pCMV-3tag6 overexpressing POMC secretome. Proteins exhibiting statistically significant ER stress-mediated differences (THA versus DMSO) in experimental groups with distinct genetic profiles for SIK2 (Control, SIK2 KD, and SIK2 WT) were evaluated. Furthermore, differences contingent on SIK2 manipulation (e.g., SIK2 KD versus Control) in ER stress or non-stress conditions were also calculated. The LFQ-based relative abundance values are listed in Table 2 and Table S1.

The heat maps were constructed for the purpose of illustrating hierarchical clusters with a comparative analysis, utilizing PD, with the distance function set to “Euclidean,” which computes the geometric distance between two data points in multidimensional space. The linkage method was set to “Complete,” which calculates the dissimilarity between two clusters as the maximum distance between any two data points in different clusters (farthest neighbors). Gene Ontology (GO) term and

biological pathway enrichment analyses were conducted using the ShinyGO software [37] with the following parameters: the database was set to GO terms (biological process, molecular function, and cellular component), and KEGG, Reactome, and WikiPathways were designated as the source of terms and pathways, respectively. Additionally, the pathway size was set to a minimum of 2 and a maximum of 5,000 genes. ClueGO (v.2.5.10) software, a Cytoscape plug-in [42], was used to determine and functionally visualize the nonsuperfluous biological terms for the resulting hierarchical clusters of genes in a functionally grouped network. The selection threshold was set to "medium", i.e., at least 3 genes from the uploaded list and 4% of genes selected for gene ontology terms were found to be associated with a term by referencing the GO term and pathway databases illustrated in the corresponding figure. The shared genes are also displayed as functional groups of terms and pathways based on a kappa score of 0.4, allowing detailed pathway analysis using the CluePedia extension. The minimum p values were calculated using the FDR method derived from the hypergeometric distribution and Bonferroni step-down statistical options. STRING [43] was used to visualize a network of protein-protein interactions in functionally related groups concerning experimental or database-predicted information. All comparative analysis cut-off was adjusted to 0.05 for p-value.

Immunoblotting and cell viability experiments were also carried out with samples from at least three independent biological replicates ( $n=3$ ). Western blot quantification was conducted using the ImageJ software (version 1.48, USA) for densitometric measurements. All statistical analyses were performed using GraphPad Prism software (version 9.3, USA). One-way ANOVAs were conducted to compare the control and treated/manipulated groups, using Bonferroni post-tests for multiple comparisons. The resulting data are presented as mean  $\pm$  standard deviation. The statistical parameters are provided in the figures and figure legends. In the process of writing the article, Scite.ai [44], an artificial intelligence-based program, was employed for the current literature review, particularly for the introduction section.

**Table 2.** SIK2 and early phase ER stress-dependent Relative Fold Changes of three major clusters.

	Accession ID	Protein Name (Abbreviation)	FDR Class*	HeatMap Cluster	Relative Abundance Ratio						
					6hr ER stress response (THA/DMSO) <sup>a</sup>			6hr Stress independent (DMSO)		6hr Stress dependent (THA)	
					Ctrl	KD	WT	KD/Ctrl <sup>b</sup>	WT/Ctrl <sup>c</sup>	KD/Ctrl <sup>b</sup>	WT/Ctrl <sup>c</sup>
Obesity and Feeding Behavior	O35082	Klotho (Kl)	Low	C1-C5	1,402	100	1,046	1,174	100	100	17,604
	O543L5	Antithrombin-III (SerpinC1)	Medium	C1-C5	1,026	1,652	0,648	0,97	1,84	2,225	1,238
	O620L7	Growth/Differentiation Factor 15 (Gdf15)	Low	C2-C5	1,645	2,185	1,133	0,671	4,022	2,455	1,968
	O62361	Pro-thyrotropin-releasing hormone (Trh)	Low	C2-C5	0,01	1,036	0,786	1	1	100	100
	E72MY9	Erythropoietin (Epo)	Low	C2-C4	18,99	0,01	12,678	9,996	1	0,068	0,969
	E2MWN9	Calreticulin (Calr)	High	C1-C5	4,119	0,468	11,924	0,45	0,917	0,178	3,571
	P12023	Amyloid-beta precursor protein (App)	Medium	C2-C5	0,965	2,27	0,706	0,498	3,189	3,072	1,518
	P15379	CD44 antigen (Cd44)	High	C1-C4	0,596	2,069	0,897	2,002	0,567	5,964	1,285
	O71LX8	Heat shock protein HSP90-beta (Hsp90abr1)	High	C3-C5	1,208	2,398	0,651	0,827	4,802	2,361	1,833
	O821P8	Angiotensin-related protein 4 (Angptl4)	Low	C2-C5	1,126	1,136	1,238	7,973	12,277	7,305	4,612
	P12032	Metalloproteinase inhibitor 1 (Timp1)	High	C2-C4	0,127	0,36	0,073	0,373	4,778	1,626	2,862
	P25785	Metalloproteinase inhibitor 2 (Timp2)	High	C2-C5	0,611	1,144	0,276	0,733	4,885	1,374	1,454
	O35988	Syndecan-4 (Sdc4)	Medium	C1-C5	0,376	0,313	0,56	0,318	1,542	0,212	1,098
	O6NCU4	SPARC (Sparc)	High	C2-C6	0,055	0,187	0,037	0,789	1,654	2,794	1,032
	AOA338P7H5	Alpha-2-HS-glycoprotein (Ahsg)	High	C3-C5	0,975	1,519	0,916	0,467	2,74	2,549	2,523
	O640N1	Adipocyte enhancer-binding protein 1 (Aebp1)	High	C2-C4	0,01	0,01	0,021	0,711	14,224	0,01	9,171
O69029	Matrilin-4 (Matn4)	Low	C1-C6	0,767	2,938	0,788	0,804	1,616	2,458	1,914	
O602F2	Glypican-1 (Gpc1)	Medium	C2-C6	0,01	0,01	0,345	0,01	1,181	0,01	12,076	
P70275	Semaphorin-3E (Sema3e)	Low	C2-C5	7,148	1,32	0,869	1,519	4,832	1,366	4,177	
O602L9	Dickkopf-like protein 1 (Dkk1)	Low	C2-C4	0,452	4,363	0,01	6,27	1	17,097	0,01	
P10605	Cathepsin B (Ctsb)	High	C3-C6	0,128	0,283	0,079	0,754	1,737	1,884	1,065	
AOA02JE75	Bone morphogenetic protein 3 (Bmp3)	Low	C3-C5	0,964	8,54	1,566	0,348	0,731	3,47	3,068	
P20722	Bone morphogenetic protein 6 (Bmp6)	Low	C1-C6	1,142	3,508	0,708	1,929	0,406	0,872	0,359	
P11087	Collagen alpha-1(I) chain (Col1a1)	High	C2-C4	0,238	0,552	0,292	0,994	2,571	4,522	2,359	
O01149	Collagen alpha-2(I) chain (Col1a2)	High	C2-C5	0,367	0,576	0,251	0,83	4,04	4,526	3,055	
O04857	Collagen alpha-1(VI) chain (Col1a1)	High	C2-C6	0,836	2,229	0,604	0,329	0,964	1	0,891	
B1B0C7	Perlecan (heparan sulfate proteoglycan 2)(Hspg2)	High	C1-C6	0,267	1,066	0,103	0,673	1,529	2,135	0,598	
P10493	Nidogen-1 (Nid1)	High	C2-C4	0,121	0,342	0,104	0,593	3,745	3,005	2,665	
O69E95	High mobility group protein B1 (Hmgb1)	Medium	C2-C5	1,027	1,904	0,787	0,633	1,679	3,271	1,944	
P34884	Macrophage migration inhibitory factor (Mif)	High	C2-C4	0,721	2,153	0,817	0,864	2,139	5,431	3,303	
O35188	Fractalkine (Cx3cl1)	Medium	C1-C6	0,882	2,532	0,596	0,549	1,786	2,366	1,016	
O6R460	Interleukin-36 gamma (Il36g)	Medium	C1-C6	1,131	2,242	0,662	0,791	1,432	2,021	1,937	
O9CP74	Myeloid-derived growth factor (Mydof)	High	C2-C4	29,652	24,199	26,057	1,423	1,431	1,28	1,348	
O4FJ4	Annexin (Anxa1)	Medium	C2-C5	0,068	0,966	0,01	0,087	0,084	1,578	0,01	
O644Y8	Granulin (Gm)	High	C2-C6	0,417	1,921	0,267	0,689	6,055	2,43	1,878	

\* FDR class, High and Medium:  $q$  value  $< 0,05$ ; Low:  $q$  value  $> 0,05$ . a: The abundance of secreted proteins in ER stressed cells compared to that of unstressed cells. b: The abundance of secreted proteins in SIK2 knockdown cells compared to control cells. c: The abundance of secreted proteins in SIK2 overexpressing cells compared to control cells.

### 3. Results

#### 3.1. Establishment of the POMC Model for Comparative Secretome Analyses

POMC neurons are the primary target of hypothalamic inflammation in diet-induced obese animal models and human subjects. Chronic exposure to dietary saturated fatty acids (SFAs) in these model organisms results in persistent ER stress and diminished autophagy flux in POMC neurons, which are repeatedly associated with neuronal loss and/or the development of leptin and insulin resistance. Taken together, the early activation of SIK2 in ER-stressed POMCs and its positive regulatory roles in ERAD and autophagy encouraged us to determine whether the regulatory role of SIK2 in these biological processes, which are tightly associated with the vesicular secretion machinery, has any effect on the cell secretome. To gain further mechanistic insight into the systemic effect of SIK2 on organismal energy homeostasis and feeding behavior, we sought to identify proteins responsible for the secretome of ER-stressed POMCs, the most salient feature of hypothalamic obesity. To achieve this goal, we designed an LC-MS/MS-based differential secretome study of the conditioned media of ER-stressed POMCs lacking or overexpressing SIK2. Prior to the start of comparative secretomic studies, the efficiency of SIK2 knockdown and overexpression in POMCs and their responsiveness to thapsigargin were confirmed by immunoblotting using specific antibodies (**Figure 1A and C**). SIK2 appears to be a highly sensitive ER stress sensor because it responded instantaneously to thapsigargin treatment, with its active form reaching a maximum in 15 min and decreasing sharply below the control level within 3 hours despite persistent stress induction and remaining relatively unchanged thereafter (**Figure 1B**). For the secretomics studies, cultured POMC cells with either endogenous, over, or underexpressed SIK2 were exposed to thapsigargin for 6 or 12 hours in the absence of serum. Secretomes subjected to 24 hours of ER stress induction were excluded from the data analyses due to the reduced proliferation and viability of the neurons (**Supplementary Figure S1A**). The percentage of viable cells present in serum-containing and serum-free cultures did not exhibit a statistically significant difference. Cell viability was persistently sustained at a level exceeding 90% (**Supplementary Figure S1B**). Also, a notable effect on cell viability or proliferation was not observed with SIK2 manipulation. The respective secretomes were collected from the conditioned media via a serial centrifugation. For the confirmation of secretome purity, immunoblotting for  $\beta$ -actin and  $\alpha$ -tubulin cytoplasmic proteins was performed on secretome samples and full proteomes. A small amount of  $\beta$ -actin was detected in the secretome samples compared to the total lysate (**Figure 1D**). Although a 12-hour time window is a commonly used interval that allows cells to synthesize their de novo secretomes, we also collected secretomes at 6 hours post-ER stress induction to more accurately represent changes attributable to SIK2 activity (peak level in the initial 30 minutes) in the resulting secretome. (**Figure 1B**). Furthermore, corroborating reports have indicated that cultured cells can produce a secretome effectively and at sufficient levels within 6 hours following treatment with pharmacological agents [45].

#### 3.2. LC-MS/MS-Based Analysis of POMC Secretomes

The secretome samples were analyzed by one-dimensional gel electrophoresis (1DE) and SYPRO-Ruby staining prior to mass spectrometry analysis. As anticipated, the buildup effect on the total secretome was noticeable at 12 hours of ER stress induction. The differential expression of some secreted proteins could even be spotted on the gel by the naked eye (**Supplementary Figure S1C**). We detected 1306 total proteins that matched the *Mus musculus* protein databank with an FDR above 0.05 and a confidence interval ranging from medium to high. Among these proteins, 149 were soluble secreted proteins, 12 were shed proteins, and the rest were intracellular proteins. To detect low abundance proteins, we used msAmanda and spectral clustering, which led to the identification of additional proteins, resulting in a final list of 885 soluble and secreted, 144 shed proteins (**Figure 2A**). Based on the LFQ abundance intensities, a heatmap was constructed, and subsequently, we applied clustering methodology to these 1029 proteins (885 soluble secreted and 144 shed) whose secretion **were either** increased or decreased together with respect to the SIK2 and ER stress variables. These hierarchical clusters of the POMCs secretome presented on the heatmap indicate differentially

regulated proteins affected by SIK2 availability in the background of 6 and 12 hours of ER stress conditions to differentiate the early and late response proteins relative to control in the secretome, respectively (**Figure 2B and C**). In the absence of ER stress, SIK2 overexpression produced the most significant ( $\geq 2$ -fold) increase in a group of related proteins (cluster 3) compared to SIK2 knockdown or control cells (**Figure 2B**). However, in response to 6 hours of ER stress induction, significant increases of at least two-fold in the secreted proteins listed in clusters 5 and 6 were detected in SIK2 knockdown cells compared to both control and SIK2 overexpression. That is ER stress-mediated SIK2 activation in POMCs suppresses the level of these proteins, especially during the early phase of ER stress response (**Figure 2C**). The comparative analyses of heatmap clusters revealed that SIK2 plays a pivotal role in regulating the secretion of proteins, particularly in the extracellular matrix, immune response, axon guidance and neurite outgrowth, and feeding behavior related terms and pathways. These findings were exclusively observed in the early phase (6 h) of the ER stress response and appear to be discharged from this duty by the implementation of late (12 h) ER stress. Although the observed fluctuations between the 6-hour and 12-hour time points in the control group in the absence of stress may be attributed to the potential effects of serum starvation, there is no statistically significant differences were calculated according to LFQ-based analysis. On the other hand, the data showed that the proportion of differentially secreted proteins showing an increase at the 6-hour time point was greater than that observed at the 12-hour time point for both SIK2 knockdown and overexpressing cells compared to the control. (**Supplementary Figure S2**). For example, SIK2 overexpression produced a broader (~70%) yet contrasting incremental effect on these secreted proteins in clusters under no stress conditions (**Supplementary Figure S2C**). Taken together, the data presented suggest that the effect of SIK2 on the POMC secretome is limited to the early phase of the ER stress response and is manifested by its ability to suppress various biological processes.

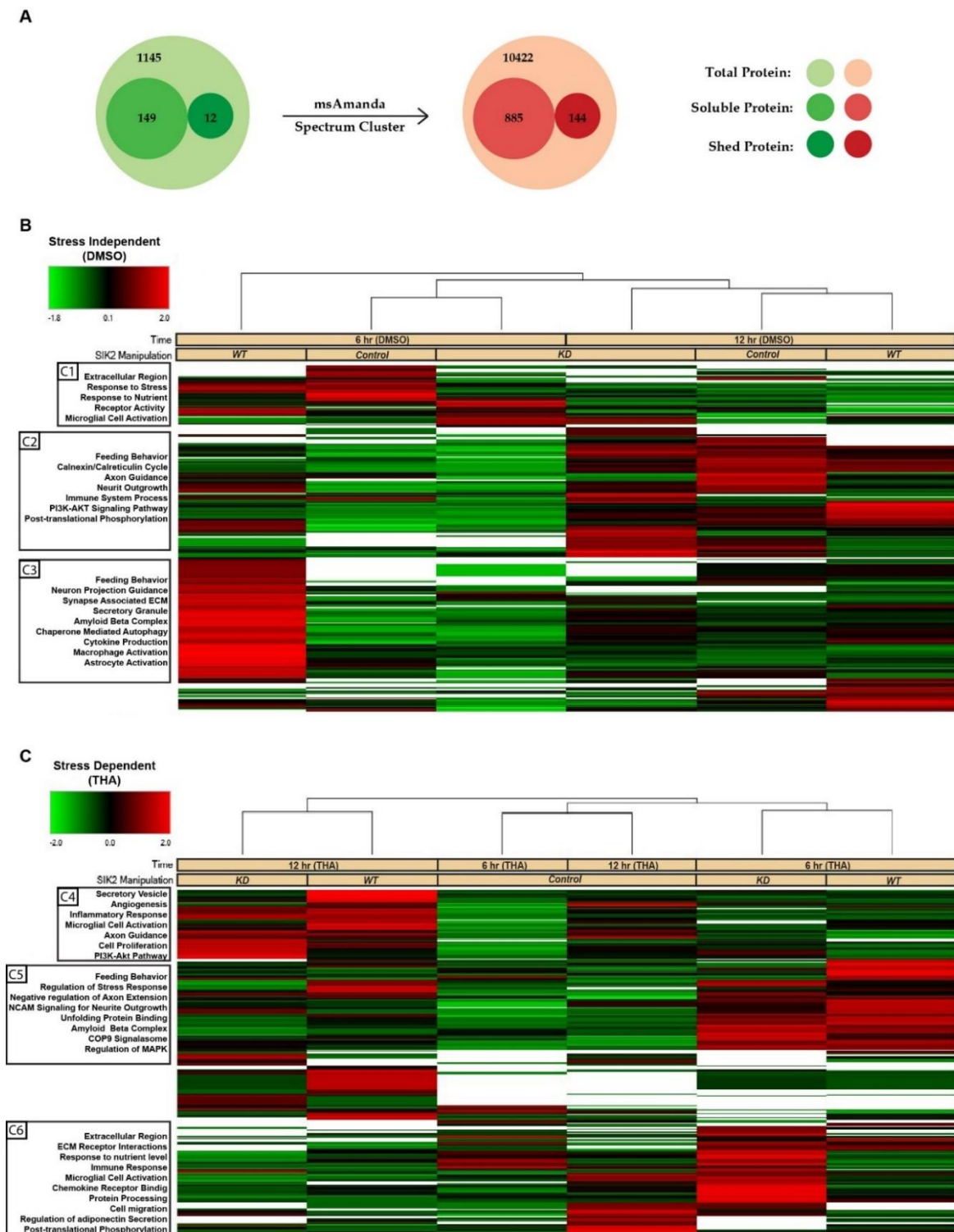


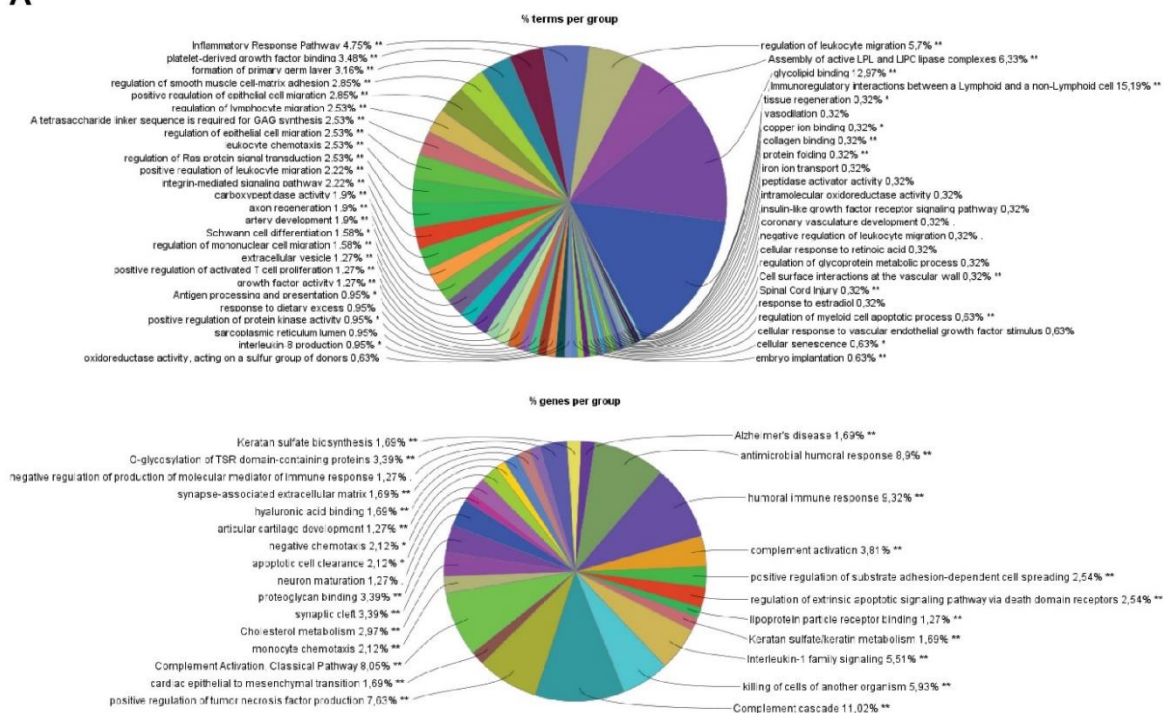
**Figure 2. Visualization of the differentially secreted POMC proteins.** A) Soluble secreted and potentially shed proteins are indicated. The radius of the circles corresponds to the number of proteins. After further iteration using MS Amanda 2.0 and spectral clustering, the resulting protein counts are shown on the right side. Heatmap of POMC secretome proteins across SIK2 manipulations in the absence (B) and presence of ER stress (C) from hierarchical clustering using Proteome Discoverer 2.3. The rows represent the proteins, and the columns indicate groups of replicates. The ratio of protein abundances was represented by a color code indicating z-scores (green shows the decrease; black shows no change; red shows the increase), as illustrated in the accompanying legend. Functional annotation clustering with ShinyGO for the gene ontology terms/pathways is shown on the left, sorted by enrichment FDR score ( $< 0.05$ ).

### 3.3. Functional Enrichment of the SIK2 and ER Stress-Derived Secretome

Functional enrichment analyses were performed on gene lists obtained from the hierarchically clustered proteins (Cluster 1-6) of the heatmap with respect to the SIK2 and ER stress variables using ShinyGO for analysis and identification of functional pathways and biological processes with the highest confidence (FDR < 0,05) (**Figures 2B and 2C**). In parallel, four clusters (Cluster 2 and 3, and Cluster 4 and 5) exhibit the SIK2 effect with greater discernibility on the heat map and have been assigned lower FDR values by ShinyGO and were transferred to ClueGO, a Cytoscape plug-in for further analysis. The nonredundant biological terms in the functionally grouped networks were evaluated using the Gene Ontology (Biological Process, Molecular Function, and Cellular Component), KEGG, Reactome, and WikiPathways databases of ClueGo (**Figures 3 and 4**).

The majority of secreted proteins are associated with cellular processes, including the cellular response to external stimuli and biological regulation of the extracellular matrix. However, the percentage distribution of secreted proteins among the functionally related groups seemed to be significantly affected by SIK2 manipulations under physiological and ER stress conditions (**Figures 3A and 4A**). In agreement with its systemic knockout phenotype, anti-inflammatory effects on macrophages, and cell survival effects on neurons and microglia, the effects of SIK2 on the identity and quantity of secreted proteins revealed the enrichment of functionally associated neuropeptides related to feeding behavior, cellular stress, and immune response, as well as neuron maturation and axon guidance in the absence of ER stress (**Figure 3B**). Furthermore, the secretion of chemotactic, inflammatory, appetite, and protein folding-associated proteins was altered by SIK2 under ER stress conditions (**Figure 4B**). Based on the LFQ abundance ratios, we identified 35 SIK2-regulated secreted proteins from the networks that are associated with obesity and feeding behavior, inflammation, and axon guidance and neurite outgrowth pathways (see **Table 2** and **Supplementary Table S1** for the complete lists).

A



B

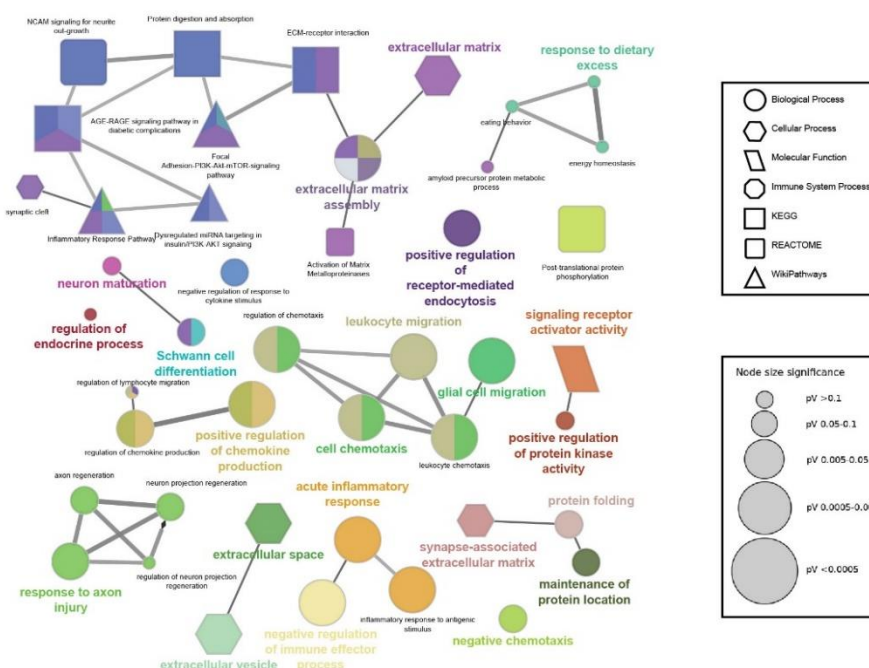


**Figure 3. Stress-independent functional enrichment analysis of the SIK2-modified POMC secretome** A) Pie charts generated by ClueGO and CluePedia showing the Gene Ontology terms and pathway analysis belonging to Cluster 2 (top) and Cluster 3 (bottom) with the percentage of terms/pathways per associated gene group. B) Network analysis of selected functionally grouped terms/pathways. Each node represents a GO term/pathway, and the node size refers to the p-value, represented by a different node shape for each database (see legend for node size and shape). The edge represents the connection between the functionally related processes (according to kappa statistics). The different colors within the same node refer to the percentage of genes that were significantly enriched within the term belonging to the different groups.



Upon analysis of these proteins, interestingly, during the early phase of the ER stress response (6 hr), a group of proteins related to feeding and energy homeostasis, including growth/differentiation factor 15 (Gdf15), Serpinc1, amyloid precursor protein (App), TIMP metalloproteinase inhibitor 1 and 2 (Timp1 and Timp2), were significantly increased in the secretome of SIK2-knockdown neurons. Surprisingly, a similar effect was reproduced, albeit to a slightly greater extent, by overexpressing SIK2 only in the absence of ER stress induction. This finding is compatible with the idea that SIK2 controls the level of these POMC-derived neuropeptides to communicate with cells in their immediate surroundings and with secondary neurons in the feeding circuitry under both physiological and early ER stress conditions. Conversely, one of the members of this group, calreticulin (Calr) decreased in SIK2-deficient POMCs in response to early ER stress induction, and this effect was reversed upon SIK2 overexpression, indicating differential regulation of counteracting factors within the same group (**Table 2**, see the obesity and feeding behavior group, red colored).

In addition, the secretion of axon guidance-related proteins, namely, perlecan (Hspg2), dickkopf-like protein 1 (Dkk1), cathepsin B (Ctsb), matrilin-4 (Matn4) and nidogen-1 (Nid1) were induced collectively in the secretome of SIK2-depleted cells in response to early ER stress induction, and similar to SIK2 overexpression in feeding and obesity-related group, SIK2 overexpression increased the secretion of these proteins in a stress-independent manner, except for Dkk1. In contrast to the general trend of other members of the group, the Dkk1 level decreased with SIK2 overexpression during the early ER stress response (**Table 2**, see the axon guidance and neurite outgrowth group, green colored).

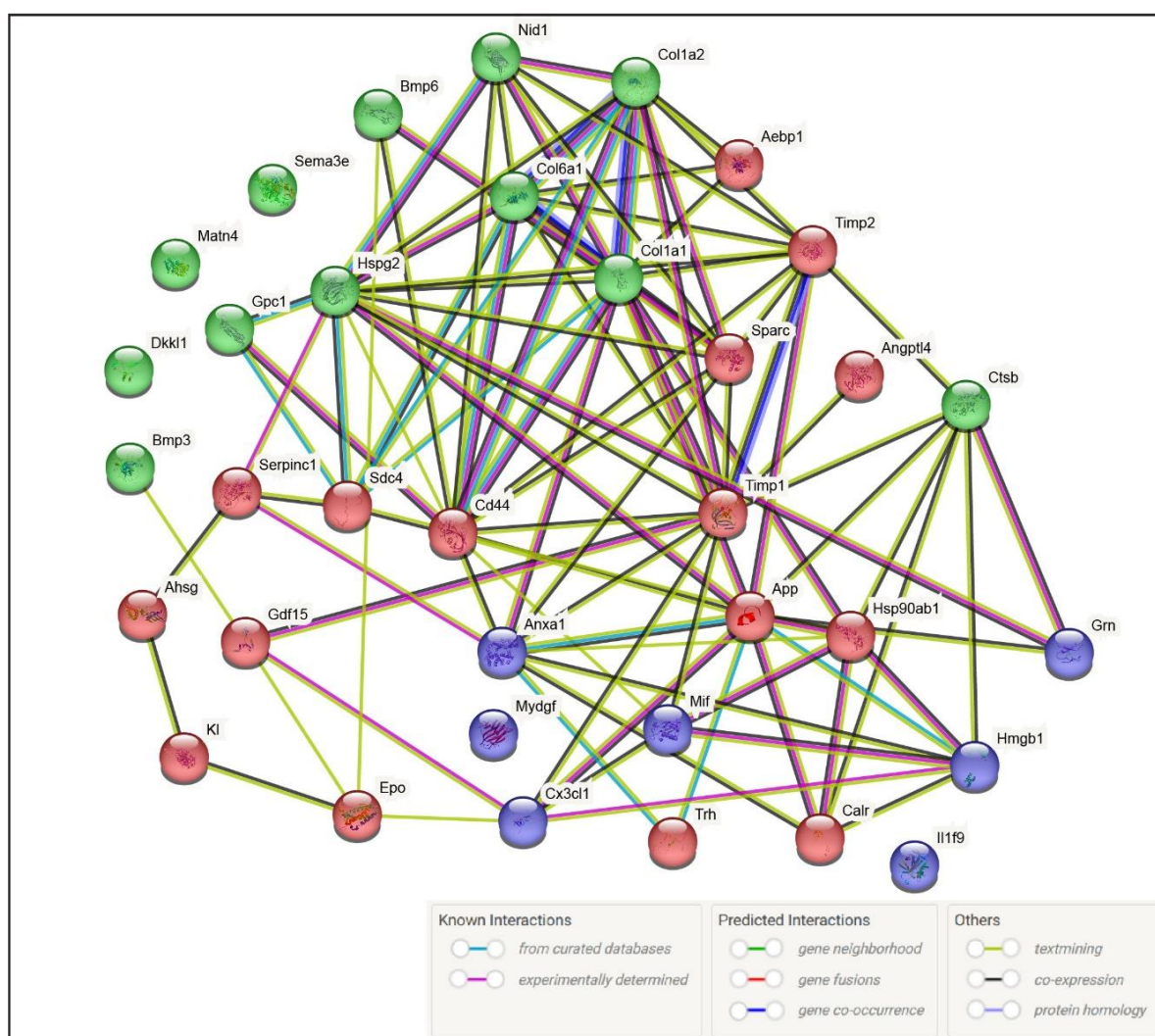
The third group of secreted proteins, which are tightly controlled by SIK2 under physiological and early ER stress conditions, belongs to the proinflammatory cytokine and chemokine family. In fact, following early ER stress induction, the expression profiles of members of this inflammatory gene group were similar to previously mentioned ones. The levels of macrophage migration inhibitory factor (Mif), annexin A1 (Anxa1), fractalkine (Cx3cl1), and granulins (Grn) in this inflammatory group were consistently and significantly upregulated in secretome POMCs lacking SIK2 upon early ER stress induction. As noted for the members of the former two groups, SIK2 had a positive effect on the levels of three inflammatory secreted proteins, Mif, Grn and Cx3cl1 in the absence of ER stress but negatively regulated Anxa1 under early ER stress conditions (**Table 2**, see the inflammation group, blue colored).

As a general trend, the levels of all these proteins listed in the three groups are confined to the early phase of the ER stress response by stress-activated SIK2, and its deactivation during the late ER stress period releases these molecules, which apparently marks the end of the cell survival period (**Supplementary Table S1**). Furthermore, functional enrichment analysis of differentially secreted proteins grouped into clusters 2 and 4 (**Figure 2B and 2C**) revealed a concerted effort to activate the major survival-related PI3K-AKT pathway during the early phase of the ER stress response [46] (**Supplementary Figure S3**), whereas death-related CHOP signaling emerged as the activity of SIK2 decreased in response to prolonged ER stress induction [47].

#### 3.4. Protein-Protein Interaction Network Analyses

A list of POMC-derived secreted proteins regulated by SIK2 during the **early** phase of the ER stress response was directly uploaded to STRING software for protein-protein interaction (PPI) network analysis (**Table 2**). A network of PPIs among functionally related proteins was visualized along with their functional annotations with reference to experimental or database-predicted information. String analysis revealed both inter- and intraconnections between the members of the three distinct gene groups obtained from the functional enrichment analyses, and the genes depicted in the PPI network are listed in the table below (**Figure 5**). Notably, PPI network analyses revealed an intricate interaction network between the members of three functionally related groups, accounting for their coregulation by SIK2, presumably downstream of the unfolded protein response (UPR), in ER-stressed POMC neurons. For example, the stress alarmone and anorectic protein Gdf15 interact with members of two other groups, including inflammatory Cx3cl1, axon guidance-related protein (Bmp3), and the obesity-related proteins Timp1 and erythropoietin (Epo). Concerning Timp1,

a shed protein implicated in the inflammatory response plays a central regulatory role at the crossroads of protein-protein interactions between obesity-related proteins and feeding behavior-related proteins (Gdf15, Cd44, Sparc and Angptl4) as well as axon guidance-related proteins (Ctsb, Hspg2, Col1a1 and 2) and neuroinflammation-related proteins (Cx3cl1, Anxa1 and Mif). We also found that cathepsin B (Ctsb), a lysosomal cysteine protease involved in protein turnover and proteolytic processing of amyloid precursor protein (APP), interacted with obesity- and feeding behavior-related proteins Calr, App, Hsp90ab1, Timp1, and Timp2 and inflammation-related Hmgb1 and Grn (**Figure 5**). Although APP is predominantly linked to the pathophysiology of Alzheimer's disease, a recent report pointed out its association with obesity phenotypes such as insulin resistance and inflammation, which are regulated by tumor necrosis factor  $\alpha$  (TNF- $\alpha$ ) [48,49]. We provided an extended and targeted evaluation of these PPIs in the discussion.



Color Code	Cluster Name	Gene Count	Protein Names
	Obesity & Feeding Behavior	16	Kl, Serpinc1, Gdf15, Trh, Epo, Calr, App, Hsp90ab1, Cd44, Angptl4, Timp1, Timp2, Sdc4, Sparc, Ahsg, Aebp1
	Axon Guidance & Neurite Outgrowth	12	Matn4, Gpc1, Sema3e, Dkk1, Ctsb, Bmp3, Bmp6, Col1a1, Col1a2, Col6a1, Hspg2, Nid1
	Inflammation	7	Hmgb1, Mif, Cx3cl1, Il1f9, Mydgf, Anxa1, Grn

**Figure 5. Illustration of protein–protein interaction network analysis using STRING.** Proteins in the PPI network are shown as 3D spheres and labeled with their respective gene names, each representing a node in the network. The nodes are connected by edges representing their interaction. The color of the edges refers to their origin of interaction knowledge as indicated. Proteins are clustered together according to their related biological terms, and each group is represented by a circle of different colors. The full names of the proteins are listed in **Table 2**.

#### 4. Discussion

Intriguingly, SIK2 localizes mainly to the ER membrane and undergoes rapid transient activation upon ER stress induction independent of its upstream activator kinase liver kinase B1 (LKB1) [50]. Although the functional importance of its ER localization and the identity of its upstream activator kinase are not fully understood, a recent study revealed that the UPR is involved in the ER stress-dependent activation of SIK2. Moreover, SIK2 has been repeatedly implicated in the regulation of major ER stress response pathways such as inflammation, ERAD, and autophagy downstream of UPR activation. SIK2 mediates the upregulation of ERAD and autophagy flux by phosphorylating p97/VCP, an unidentified factor involved in autophagosome-lysosome fusion, respectively, on the ER membrane. Consistent with these findings, a recent report proposed that SIK2 enrichment in ER lipid rafts is required for the proper packaging of secretory cargo proteins into export vesicles, suggesting a molecular mechanism that enables SIK2 to modify the level and/or identity of secreted proteins. In the same study, SIK2 was also shown to relocate to a distinct ER subdomain to promote autophagy and protect cells from apoptosis under ER stress conditions [51]. Based on the ER stress-mediated activation and localization of SIK2 to lipid rafts, we hypothesized that the effect of SIK2 on the POMC secretome could be readily delineated by probing qualitative and quantitative changes in secreted proteins via high-resolution LC-MS/MS-based secretome studies. To do so, we designed a comparative secretomic study to decipher the effects of SIK2 on the POMC secretome alone or in combination with pharmacologically induced ER stress conditions. Comparative analyses of the POMC secretomes specific to the early and prolonged phases of ER stress responses revealed the intriguing ability of SIK2 to control the expression profiles of dozens of secreted proteins concertedly only during the early phase of the ER stress response, consistent with its ER stress-dependent activation profile (Figure 1B). The functional clustering of these genes revealed six biologically relevant clusters, of which we focused on the four clusters (Cluster 2 and 3, and Cluster 4 and 5) related to obesity and feeding behavior, axon guidance and neurite outgrowth, and neuroinflammation based on their FDR values and close association with inflammation and cell survival, the cardinal biological functions of SIK2 in various cell types, including neurons and glia. Our comparative secretome analyses demonstrated that the effect of SIK2 on the POMC secretome is limited to the early phase of the ER stress response. However, prolonged ER stress uncouples SIK2 from its effectors, thereby unleashing inflammatory and apoptotic secreted mediators to execute their functions within or on distantly located neuronal and nonneuronal cells. That is, during this prolonged ER stress response, SIK2 repression of these secreted proteins, which are clustered in three different but functionally integrated groups, is relieved coincident with the deactivation of SIK2. As noted before, SIK2 suppresses the inflammatory content of the POMC secretome primarily in the early phase of the ER stress response almost identically to its effect on two other groups, including obesity and feeding behavior, axon guidance and neurite outgrowth (Table 2).

The early phase-specific profile imposed on SIK2 availability is commonly observed with the members of the three collectively acting groups. To avoid profile redundancy, we intentionally concentrated on a few representative secretome proteins selected from these three major groups (Figures 5 and 6). One of the most interesting proteins listed in the table related to obesity and feeding behavior is Gdf15. It is an anorexigenic protein and acts through its cognate receptor, GFRAL, on the paraventricular nucleus (PVN) downstream of POMC neurons to end feeding and increase energy expenditure [52]. In our study, the level of Gdf15 in the SIK2 knockdown POMC secretome significantly increased in response to early ER stress induction and returned to the control level in response to SIK2 overexpression. However, without ER stress, the overexpression of SIK2 caused an

increase in the Gdf15 level comparable to or even greater than that induced by ER stress in the absence of SIK2. It is commonly observed that the level of circulating Gdf15 is elevated in obese human subjects despite increased food intake [53]. Since exogenous Gdf15 injection ameliorated the obesity phenotype in obese animal models [54], therapeutic strategies targeting Gdf15 or its upstream regulator SIK2 in POMC neurons of the obese human brain will require the identification of differences in the Gdf15-GFRAL axis between the two species. In this group, calreticulin (Calr), which responds to early ER stress induction, exhibited a twofold increase in the secretome of SIK2-overexpressing neurons compared to that of control neurons. Accordingly, the level of Calr decreased significantly with SIK2 deficiency independent of ER stress, in stark contrast to other members of the same group, excluding the coregulated proteins of other groups. Calreticulin is a multifunctional ER chaperone implicated in obesity and related metabolic disorders, and its secreted form acts as a molecular chaperone for App [55,56]. It has been implicated in several aspects of obesity and feeding behavior in addition to its well-known role in the pathophysiology of Alzheimer's disease [48]. We presumed that the reduced low level of Calr detected in the secretome of SIK2-deficient POMC neurons during the early ER stress response may interfere with the proper folding of App in relation to the pathogenesis of obesity and related diseases.

Cd44 antigen is a transmembrane protein expressed in both glial and neuronal cells, and its depletion has been linked to inflammation, neurite outgrowth, insulin resistance, and resistance to high-fat diet-induced obesity [57–59]. The level of Cd44 in the POMC secretome undergoes dynamic changes with respect to ER stress and SIK2 availability, which is in complete agreement with the findings of the gate-keeper model imposed by the absence of SIK2 during the early response phase of ER stress induction. However, SIK2 overexpression in POMCs caused a significant decrease in the Cd44 level, contrary to otherwise coregulated members of this and other related groups, especially those with no ER stress. Collectively, these results substantiated the anti-inflammatory and regulatory role of SIK2 in axonal guidance by decreasing the level of Cd44 in the secretome, thereby aggravating disease pathogenesis in its absence. Perlecan, a heparan sulfate proteoglycan, has been demonstrated to play a role in neuronal development and neurite outgrowth, with evidence supporting its involvement in brain repair following injury [60]. The level of perlecan in the SIK2 knockdown POMC secretome significantly increased in response to early ER stress induction and decreased in response to SIK2 overexpression. However, without ER stress, the overexpression of SIK2 caused an increase in the perlecan level comparable to that induced by ER stress in the absence of SIK2.

Fractalkine/Cx3cl1, a selected member of the inflammatory group, responds collectively with other members of the group to the gatekeeper molecule SIK2, which is a chemokine that plays a critical role in modulating neuronal–microglial communication [61,62]. It has a dual role in neuroinflammation, inhibiting the production of proinflammatory cytokines by microglia while acting as a chemoattractant for immune cells [63,64]. In agreement with the proposed model for the role of SIK2 in dictating early phase ER stress responsiveness of the POMC secretome, the Cx3cl1 level was increased 2-2.5-fold in POMC knockdown cells, and SIK2 overexpression reversed this increase in the early phase of the ER stress response. However, in the absence of ER stress, SIK2 overexpression increased the level of Cx3cl1, contrary to its absence. This indicates that the ability of SIK2 to suppress fractalkine levels in the POMC secretome during the early phase of the ER stress response is dependent on its UPR-mediated activation. Nevertheless, in the absence of ER stress, SIK2 is inactive and may act as a dominant negative to block endogenous SIK2 activity due to the tonic physiological level of ER stress. Granulin, a marker of chronic inflammation associated with insulin resistance, obesity, and type 2 diabetes mellitus, and its expression profile in the POMC secretome also obeyed the regulatory constraint imposed by a gatekeeper function of SIK2 [65]. For the extended coverage of the quantitative changes in the members of the three major groups, readers are referred to **Table 2**.

Overall, we propose a *gatekeeper* model for SIK2 because of its ability to maintain the transient control of these otherwise pathologically relevant inflammatory and apoptotic pathways during the early phase of the response to ER stress induction and to provide cells with a window of opportunity to rectify ER stress and maintain organismal homeostasis and cellular survival. In other words, SIK2

acts as a stopcock for the uncontrolled surge of double-edged biological processes such as inflammation and autophagy at the physiological level to maintain neuronal functions and survival. In contrast, prolonged unresolved ER stress tips the balance toward pathologically relevant chronic inflammation and abrogates autophagy by dampening the activity of SIK2, which agrees well with our data-driven *gatekeeper* model depicted in **Figure 6**. Although the molecular mechanisms responsible for the SIK2-mediated changes in the levels of secreted proteins are not addressed here, we propose that SIK2 could achieve this indirectly by regulating ERAD and autophagy processes or directly by modulating the autophagy-related unconventional secretion pathway. The effect of SIK2 on POMC secretome profiles during early ER stress response can be mediated either at the transcriptional level by modulating the activity of its downstream coactivators CREB-regulated transcription coactivators (CRTCs), p300/CREB-binding protein, and transcription factor EB (TFEB) or by upregulating ERAD and autophagy fluxes, respectively [17,66]. However, it is equally or even more likely that SIK2 participates in the coat protein complex II (COPII) vesicle formation and/or cargo selection at the specified ER subdomains rich in lipid rafts [67]. Our laboratory and others reported direct and indirect physical interactions between SIK2 and the outer coat protein of COPII vesicles in immunoprecipitation-based mass spectrometry (IP-MS)-driven protein-protein interaction data (unpublished data). Based on the localization of SIK2 to lipid rafts on the ER membrane where COPII vesicles form, we speculated that SIK2 in lipid rafts could regulate either the formation of secretion vesicles or the selection of cargo proteins for secretion [50,67].

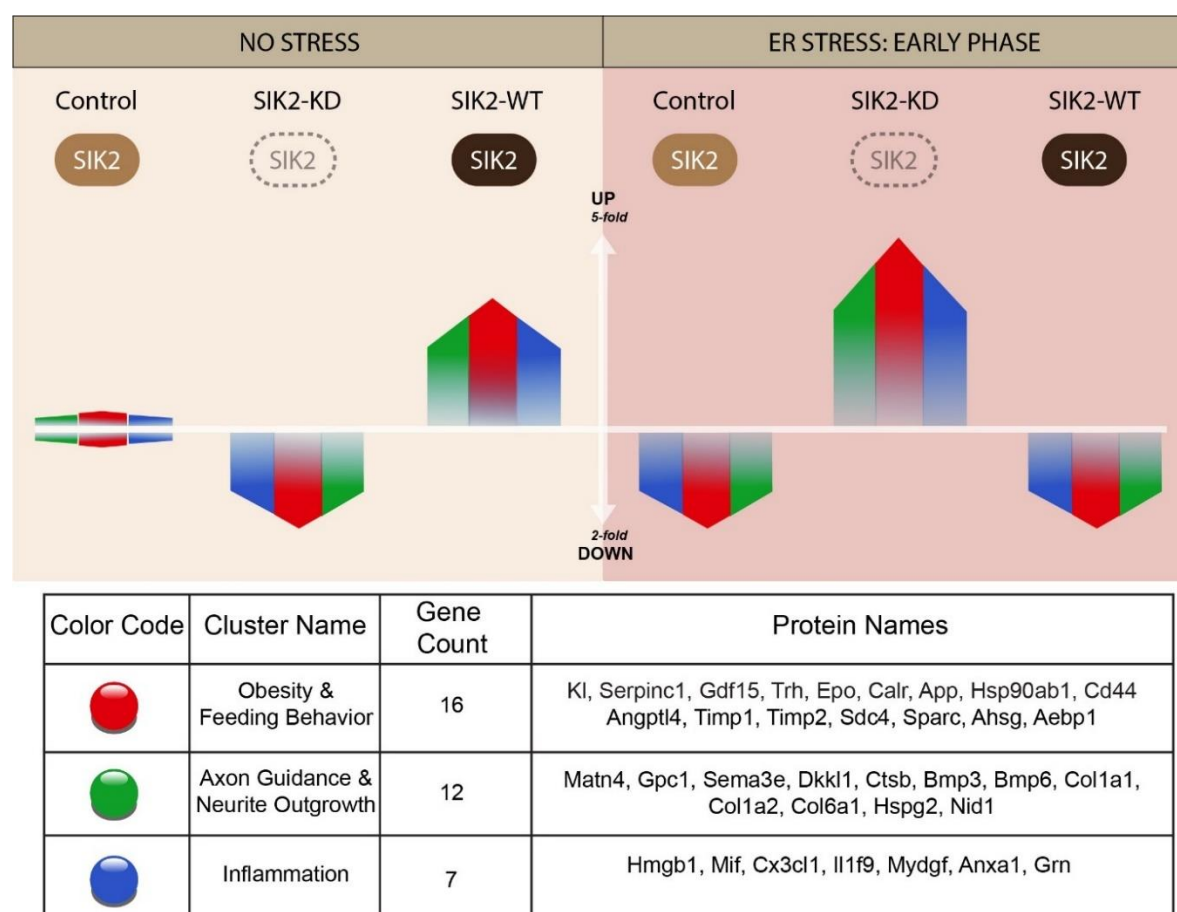


**Figure 6. Differential and synergistic effects of SIK2 and ER stress on selected proteins of three major clusters.** Relative fold changes are represented by colored bar according to their correlation with the differential gene expression (DGE) pattern. The bars illustrate the relative increase or decrease in secreted proteins. Protein abundance in all experimental conditions was normalized to the control group in the absence of stress. An extended list of relative fold changes for the genes excluded from the graph is provided (see **Table 2**).

The novel aspect of the proposed work lies in undertaking the issue of obesity pathogenesis by examining the secreted neuropeptides and neurotransmitters of pathologically relevant POMC neurons, the central control unit for organismal energy homeostasis and energy expenditure. In diet-induced obese (DIO) animal models and human subjects, POMC neurons are either malfunctioning (resistant to anorectic hormones such as leptin and insulin) or depleted due to apoptotic loss. Therefore, the maintenance of healthy communication with their immediate neighbors (i.e., microglia, astrocytes, etc.) and distantly localized secondary neurons in the feeding circuitry (PVN) through their secreted proteins is vital for POMCs and thereby the life of an organism. We proposed an unprecedented regulatory role for SIK2 in the homeostatic control of obesity-related secreted proteins within physiological boundaries in response to the early phase of ER stress conditions. However, if unmitigated, persistent ER stress will unlock the SIK2 gate to allow a sudden increase in the levels of these obesogenic genes, which is compatible with disease pathogenesis. As noted in our model (**Figure 6**), when SIK2 was overexpressed, SIK2 could reverse this inflammatory state, although additional studies are needed to determine the effective dose for enhancing SIK2 activity due to the possibility of eradicating the basal response to ER stress.

In this study, we identified a number of POMC-driven pathologically relevant secreted molecules that we believe could be targeted individually or in combination to combat obesity and related diseases. It would be quite interesting and informative to obtain molecular insight into the possible regulatory roles of SIK2 both in the formation and cargo selection processes of secretory autophagosomes and COP II vesicles. Our comparative secretomic study revealed dozens of therapeutically valuable target proteins secreted by POMC neurons to modulate the immediate surroundings of neuronal and nonneuronal cells along distantly located secondary neurons of the PVN, all of which are implicated in the etiology and pathogenesis of obesity and various associated metabolic diseases, including neurodegeneration.

**Supplementary Materials:** The following supporting information can be downloaded at the website of this paper posted on Preprints.org, Figure S1: Evaluation of cytotoxicity and cell viability against stress conditions, and quality control of POMC secretomes; Figure S2: Heatmaps for ER stress responses specific to SIK2 manipulations; Figure S3: PI3K-AKT pathway with detected proteins according to the KEGG database; Table S1: SIK2 and prolonged ER stress-dependent relative fold changes of three major clusters.

**Author Contributions:** Conceptualization, F.Ö., M.S.T. and A.Y.; methodology, F.Ö., M.S.T. and A.Y.; validation, M.S.T. and A.Y.; formal analysis, F.Ö., M.S.T. and A.Y.; investigation, M.S.T. and A.Y.; data curation, F.Ö., M.S.T. and A.Y.; writing—original draft preparation, F.Ö., M.S.T. and A.Y.; writing—review and editing, F.Ö., M.S.T. and A.Y.; visualization, M.S.T. and A.Y.; supervision, F.Ö.; project administration, F.Ö. All authors have read and agreed to the published version of the manuscript.

**Funding:** This research was funded by TUBITAK, grant number 122Z021.

**Data Availability Statement:** Data are available upon request by qualified researchers to the corresponding author.

**Acknowledgments:** All figures are designed by Mehmet Soner Türküner using Adobe Illustrator 2019.

**Conflicts of Interest:** The authors declare no conflicts of interest.

## List of Abbreviations

- SIK2:** Salt inducible kinase 2
- POMCs:** mHypoA-POMC/GFP-2 cells
- DIO:** Diet-induced obesity
- ARC:** Arcuate nucleus
- CNS:** Central nervous system
- PVH:** Paraventricular nuclei of the hypothalamus
- DMH:** Dorsomedial nucleus of the hypothalamus
- LHA:** Lateral hypothalamic area
- ALS:** Amyotrophic lateral sclerosis
- LC-MS/MS:** Liquid chromatography–mass spectrometry

**IP-MS:** Immunoprecipitation-based mass spectrometry

**PSM:** Peptide sequence mass

**LFQ:** Label-free quantification

**GO:** Gene Ontology

**FDR:** False discovery rate

**1DE:** one-dimensional gel electrophoresis

**DDA:** Data-dependent acquisition

**DGE:** Differential gene expression

## References

1. G. J. Morton, D. E. Cummings, D. G. Baskin, G. S. Barsh, and M. W. Schwartz, 'Central nervous system control of food intake and body weight.', *Nature*, vol. 443, no. 7109, pp. 289–95, Sep. 2006, doi: 10.1038/nature05026.
2. M. J. Krashes *et al.*, 'An excitatory paraventricular nucleus to AgRP neuron circuit that drives hunger', *Nature* 2014 507:7491, vol. 507, no. 7491, pp. 238–242, Feb. 2014, doi: 10.1038/nature12956.
3. Q. Tong, C.-P. Ye, J. E. Jones, J. K. Elmquist, and B. B. Lowell, 'Synaptic release of GABA by AgRP neurons is required for normal regulation of energy balance.', *Nat Neurosci*, vol. 11, no. 9, pp. 998–1000, Sep. 2008, doi: 10.1038/nn.2167.
4. C. Quarta, X. Fioramonti, and D. Cota, 'POMC Neurons Dysfunction in Diet-induced Metabolic Disease: Hallmark or Mechanism of Disease?', *Neuroscience*, vol. 447, pp. 3–14, Nov. 2020, doi: 10.1016/j.neuroscience.2019.09.031.
5. M. A. Cowley *et al.*, 'Leptin activates anorexigenic POMC neurons through a neural network in the arcuate nucleus', *Nature*, vol. 411, no. 6836, pp. 480–484, May 2001, doi: 10.1038/35078085.
6. R. M. Dores and A. J. Baron, 'Evolution of POMC: origin, phylogeny, posttranslational processing, and the melanocortins.', *Ann N Y Acad Sci*, vol. 1220, pp. 34–48, Mar. 2011, doi: 10.1111/j.1749-6632.2010.05928.x.
7. D. Wang *et al.*, 'Whole-brain mapping of the direct inputs and axonal projections of POMC and AgRP neurons', *Front Neuroanat*, vol. 9, p. 135563, Mar. 2015, doi: 10.3389/fnana.2015.00040.
8. J. Banerjee *et al.*, 'CX3CL1 action on microglia protects from diet-induced obesity by restoring POMC neuronal excitability and melanocortin system activity impaired by high-fat diet feeding', *bioRxiv*, p. 2021.11.08.467521, Nov. 2021, doi: 10.1101/2021.11.08.467521.
9. C. A. Natale *et al.*, 'Sex steroids regulate skin pigmentation through nonclassical membrane-bound receptors.', *Elife*, vol. 5, Apr. 2016, doi: 10.7554/eLife.15104.
10. S. Nasif *et al.*, 'Islet 1 specifies the identity of hypothalamic melanocortin neurons and is critical for normal food intake and adiposity in adulthood', *Proc Natl Acad Sci U S A*, vol. 112, no. 15, pp. E1861–E1870, Apr. 2015, doi: 10.1073/pnas.1500672112.
11. C. Quarta *et al.*, 'POMC neuronal heterogeneity in energy balance and beyond: an integrated view', *Nat Metab*, vol. 3, no. 3, pp. 299–308, Feb. 2021, doi: 10.1038/s42255-021-00345-3.
12. B. Coupé, Y. Ishii, M. O. Dietrich, M. Komatsu, T. L. Horvath, and S. G. Bouret, 'Loss of autophagy in pro-opiomelanocortin neurons perturbs axon growth and causes metabolic dysregulation.', *Cell Metab*, vol. 15, no. 2, pp. 247–55, Feb. 2012, doi: 10.1016/j.cmet.2011.12.016.
13. E. Kwon and Y.-H. Jo, 'Activation of the ARC POMC→MeA Projection Reduces Food Intake.', *Front Neural Circuits*, vol. 14, p. 595783, 2020, doi: 10.3389/fncir.2020.595783.
14. N. Horike *et al.*, 'Adipose-specific expression, phosphorylation of Ser794 in insulin receptor substrate-1, and activation in diabetic animals of salt-inducible kinase-2', *Journal of Biological Chemistry*, vol. 278, no. 20, pp. 18440–18447, May 2003, doi: 10.1074/jbc.M211770200.
15. J. Park *et al.*, 'SIK2 Is Critical in the Regulation of Lipid Homeostasis and Adipogenesis In Vivo', *Diabetes*, vol. 63, no. 11, pp. 3659–3673, Nov. 2014, doi: 10.2337/db13-1423.
16. T. Sasaki *et al.*, 'SIK2 is a key regulator for neuronal survival after ischemia via TORC1-CREB.', *Neuron*, vol. 69, no. 1, pp. 106–19, Jan. 2011, doi: 10.1016/j.neuron.2010.12.004.
17. F.-C. Yang *et al.*, 'Reversible acetylation regulates salt-inducible kinase (SIK2) and its function in autophagy.', *J Biol Chem*, vol. 288, no. 9, pp. 6227–37, Mar. 2013, doi: 10.1074/jbc.M112.431239.
18. Y. Liu, V. Poon, G. Sanchez-Watts, A. G. Watts, H. Takemori, and G. Aguilera, 'Salt-Inducible Kinase Is Involved in the Regulation of Corticotropin-Releasing Hormone Transcription in Hypothalamic Neurons in Rats', *Endocrinology*, vol. 153, no. 1, pp. 223–233, Jan. 2012, doi: 10.1210/en.2011-1404.
19. C. Iorio *et al.*, 'Silencing the G-protein coupled receptor 3-salt inducible kinase 2 pathway promotes human  $\beta$  cell proliferation', *Commun Biol*, vol. 4, no. 1, p. 907, Jul. 2021, doi: 10.1038/s42003-021-02433-2.
20. N. J. Darling, R. Toth, J. S. C. Arthur, and K. Clark, 'Inhibition of SIK2 and SIK3 during differentiation enhances the anti-inflammatory phenotype of macrophages.', *Biochem J*, vol. 474, no. 4, pp. 521–537, Feb. 2017, doi: 10.1042/BCJ20160646.

21. N. J. Darling, J. S. C. Arthur, and P. Cohen, 'Salt-inducible kinases are required for the IL-33-dependent secretion of cytokines and chemokines in mast cells.', *J Biol Chem*, vol. 296, p. 100428, 2021, doi: 10.1016/j.jbc.2021.100428.
22. F. C. Yang *et al.*, 'Interaction between salt-inducible kinase 2 (SIK2) and p97/valosin-containing protein (VCP) regulates endoplasmic reticulum (ER)-associated protein degradation in mammalian cells', *Journal of Biological Chemistry*, vol. 288, no. 47, pp. 33861–33872, Nov. 2013, doi: 10.1074/jbc.M113.492199.
23. G. D. Kusuma, J. Carthew, R. Lim, and J. E. Frith, 'Effect of the Microenvironment on Mesenchymal Stem Cell Paracrine Signaling: Opportunities to Engineer the Therapeutic Effect.', *Stem Cells Dev*, vol. 26, no. 9, pp. 617–631, May 2017, doi: 10.1089/scd.2016.0349.
24. M. Ghasemi, E. Roshandel, M. Mohammadian, B. Farhadhosseinabadi, P. Akbarzadehlaleh, and K. Shamsasenjan, 'Mesenchymal stromal cell-derived secretome-based therapy for neurodegenerative diseases: overview of clinical trials', *Stem Cell Res Ther*, vol. 14, no. 1, p. 122, May 2023, doi: 10.1186/s13287-023-03264-0.
25. M.-P. B, T. FG, A. SI, M. B, B. LA, and S. AJ, 'Secretome of Undifferentiated Neural Progenitor Cells Induces Histological and Motor Improvements in a Rat Model of Parkinson's Disease', *Stem Cells Transl Med*, vol. 7, no. 11, 2018, doi: 10.1002/SCTM.18-0009.
26. M. Barbosa *et al.*, 'Intrathecal Injection of the Secretome from ALS Motor Neurons Regulated for miR-124 Expression Prevents Disease Outcomes in SOD1-G93A Mice', *Biomedicines*, vol. 10, no. 9, p. 2120, Aug. 2022, doi: 10.3390/biomedicines10092120.
27. C.-X. Yi *et al.*, 'TNF $\alpha$  drives mitochondrial stress in POMC neurons in obesity', *Nat Commun*, vol. 8, no. 1, p. 15143, May 2017, doi: 10.1038/ncomms15143.
28. T. Liu, Y. Xu, C.-X. Yi, Q. Tong, and D. Cai, 'The hypothalamus for whole-body physiology: from metabolism to aging', *Protein Cell*, vol. 13, no. 6, pp. 394–421, Jun. 2022, doi: 10.1007/s13238-021-00834-x.
29. G. F. P. Souza *et al.*, 'Defective regulation of POMC precedes hypothalamic inflammation in diet-induced obesity', *Sci Rep*, vol. 6, no. 1, p. 29290, Jul. 2016, doi: 10.1038/srep29290.
30. A. Ajoolabady *et al.*, 'ER stress in obesity pathogenesis and management.', *Trends Pharmacol Sci*, vol. 43, no. 2, pp. 97–109, Feb. 2022, doi: 10.1016/j.tips.2021.11.011.
31. A. E. Rumora *et al.*, 'The Divergent Roles of Dietary Saturated and Monounsaturated Fatty Acids on Nerve Function in Murine Models of Obesity', *Journal of Neuroscience*, vol. 39, no. 19, pp. 3770–3781, May 2019, doi: 10.1523/JNEUROSCI.3173-18.2019.
32. A. Nazarians-Armavil, J. A. Chalmers, C. B. Lee, W. Ye, and D. D. Belsham, 'Cellular insulin resistance disrupts hypothalamic mHypoA-POMC/GFP neuronal signaling pathways', *Journal of Endocrinology*, vol. 220, no. 1, pp. 13–24, Jan. 2014, doi: 10.1530/JOE-13-0334.
33. E. K. Tse and D. D. Belsham, 'Palmitate induces neuroinflammation, ER stress, and Pomc mRNA expression in hypothalamic mHypoA-POMC/GFP neurons through novel mechanisms that are prevented by oleate', *Mol Cell Endocrinol*, vol. 472, pp. 40–49, Sep. 2018, doi: 10.1016/J.MCE.2017.11.017.
34. M. H. Jäntti *et al.*, 'Palmitate and thapsigargin have contrasting effects on ER membrane lipid composition and ER proteostasis in neuronal cells', *Biochim Biophys Acta Mol Cell Biol Lipids*, vol. 1867, no. 11, Nov. 2022, doi: 10.1016/j.bbalip.2022.159219.
35. Y. Sang *et al.*, 'Salt ions and related parameters affect PEI-DNA particle size and transfection efficiency in Chinese hamster ovary cells.', *Cytotechnology*, vol. 67, no. 1, pp. 67–74, Jan. 2015, doi: 10.1007/s10616-013-9658-z.
36. B. Yuan, R. Latek, M. Hossbach, T. Tuschl, and F. Lewitter, 'siRNA Selection Server: an automated siRNA oligonucleotide prediction server', *Nucleic Acids Res*, vol. 32, no. Web Server, pp. W130–W134, Jul. 2004, doi: 10.1093/nar/gkh366.
37. Addgene, 'Addgene Plasmid 10878. Protocol Version 1.0.', pLKO.1 - TRC Cloning Vector. Accessed: Jun. 06, 2024. [Online]. Available: <https://www.addgene.org/protocols/plko/>
38. Anton Posch, *Proteomic Profiling*, vol. 2261. in *Methods in Molecular Biology*, vol. 2261. New York, NY: Springer US, 2021. doi: 10.1007/978-1-0716-1186-9.
39. C. A. Schneider, W. S. Rasband, and K. W. Eliceiri, 'NIH Image to ImageJ: 25 years of image analysis', *Nat Methods*, vol. 9, no. 7, pp. 671–675, Jul. 2012, doi: 10.1038/nmeth.2089.
40. J. Griss *et al.*, 'Spectral Clustering Improves Label-Free Quantification of Low-Abundant Proteins', *J Proteome Res*, vol. 18, no. 4, pp. 1477–1485, Apr. 2019, doi: 10.1021/acs.jproteome.8b00377.
41. V. Dorfer *et al.*, 'MS Amanda, a universal identification algorithm optimized for high accuracy tandem mass spectra', *J Proteome Res*, vol. 13, no. 8, pp. 3679–3684, Aug. 2014, doi: 10.1021/pr500202e.
42. G. Bindea *et al.*, 'ClueGO: a Cytoscape plug-in to decipher functionally grouped gene ontology and pathway annotation networks.', *Bioinformatics*, vol. 25, no. 8, pp. 1091–3, Apr. 2009, doi: 10.1093/bioinformatics/btp101.
43. D. Szklarczyk *et al.*, 'The STRING database in 2023: protein–protein association networks and functional enrichment analyses for any sequenced genome of interest', *Nucleic Acids Res*, vol. 51, no. D1, pp. D638–D646, Jan. 2023, doi: 10.1093/nar/gkac1000.

44. J. M. Nicholson *et al.*, 'scite: A smart citation index that displays the context of citations and classifies their intent using deep learning', *Quantitative Science Studies*, vol. 2, no. 3, pp. 882–898, Nov. 2021, doi: 10.1162/qss\_a\_00146.
45. J. Goodman, 'Characterizing the secretome of adipose tissue in metabolic stress', 2024, doi: 10.7916/5XGQ-2917.
46. R. B. Hamanaka, E. Bobrovnikova-Marjon, X. Ji, S. A. Liebhaber, and J. A. Diehl, 'PERK-dependent regulation of IAP translation during ER stress', *Oncogene*, vol. 28, no. 6, pp. 910–920, Feb. 2009, doi: 10.1038/onc.2008.428.
47. K. Hyoda, T. Hosoi, N. Horie, Y. Okuma, K. Ozawa, and Y. Nomura, 'PI3K-Akt inactivation induced CHOP expression in endoplasmic reticulum-stressed cells.', *Biochem Biophys Res Commun*, vol. 340, no. 1, pp. 286–90, Feb. 2006, doi: 10.1016/j.bbrc.2005.12.007.
48. J. Kang *et al.*, 'The precursor of Alzheimer's disease amyloid A4 protein resembles a cell-surface receptor', *Nature*, vol. 325, no. 6106, pp. 733–736, Feb. 1987, doi: 10.1038/325733a0.
49. G. Sommer *et al.*, 'Amyloid precursor protein expression is induced by tumor necrosis factor  $\alpha$  in 3T3-L1 adipocytes', *J Cell Biochem*, vol. 108, no. 6, pp. 1418–1422, Dec. 2009, doi: 10.1002/jcb.22382.
50. C. Zhang *et al.*, 'Activation of salt Inducible Kinases, IRE1 and PERK leads to Sec bodies formation in *Drosophila* S2 cells', 2021.
51. H.-H. Wang *et al.*, 'Activation of salt-inducible kinase 2 promotes the viability of peritoneal mesothelial cells exposed to stress of peritoneal dialysis', *Cell Death Dis*, vol. 7, no. 7, pp. e2298–e2298, Jul. 2016, doi: 10.1038/cddis.2016.79.
52. L. Yang *et al.*, 'GFRAL is the receptor for GDF15 and is required for the anti-obesity effects of the ligand', *Nat Med*, vol. 23, no. 10, pp. 1158–1166, Oct. 2017, doi: 10.1038/nm.4394.
53. I. Cimino and A. P. Coll, 'The role of GDF15 in food intake and appetitive behaviour', Feb. 01, 2022, *Elsevier Ltd.* doi: 10.1016/j.coemr.2021.100299.
54. C. Hale and M. M. Véniant, 'Growth differentiation factor 15 as a potential therapeutic for treating obesity', Apr. 01, 2021, *Elsevier GmbH.* doi: 10.1016/j.molmet.2020.101117.
55. E. Jeffery, L. R. Peters, and M. Raghavan, 'The polypeptide binding conformation of calreticulin facilitates its cell-surface expression under conditions of endoplasmic reticulum stress.', *J Biol Chem*, vol. 286, no. 4, pp. 2402–15, Jan. 2011, doi: 10.1074/jbc.M110.180877.
56. R. J. Johnson, G. Xiao, J. Shanmugaratnam, and R. E. Fine, 'Calreticulin functions as a molecular chaperone for the-amyloid precursor protein', 2001. [Online]. Available: [www.elsevier.com/locate/neuaging](http://www.elsevier.com/locate/neuaging)
57. H. S. Kang *et al.*, 'CD44 Plays a Critical Role in Regulating Diet-Induced Adipose Inflammation, Hepatic Steatosis, and Insulin Resistance', *PLoS One*, vol. 8, no. 3, p. e58417, Mar. 2013, doi: 10.1371/journal.pone.0058417.
58. A. Hasib *et al.*, 'CD44 contributes to hyaluronan-mediated insulin resistance in skeletal muscle of high-fat-fed C57BL/6 mice', *Am J Physiol Endo-crinol Metab*, vol. 317, pp. 973–983, 2019, doi: 10.1152/ajpendo.00215.2019.-Extracellular.
59. J. Zhang, W. Gan, R. Peng, L. Lu, W. Lu, and J. Liu, 'Activation of the mTOR pathway promotes neurite growth through upregulation of CD44 expression.', *J Int Med Res*, vol. 51, no. 6, p. 3000605231178510, Jun. 2023, doi: 10.1177/03000605231178510.
60. A. L. Trout *et al.*, 'Perlecan Domain-V Enhances Neurogenic Brain Repair After Stroke in Mice', *Transl Stroke Res*, vol. 12, no. 1, pp. 72–86, Feb. 2021, doi: 10.1007/s12975-020-00800-5.
61. C. AE *et al.*, 'Control of microglial neurotoxicity by the fractalkine receptor', *Nat Neurosci*, vol. 9, no. 7, 2006, doi: 10.1038/NN1715.
62. S. Castro-Sánchez, Á. J. García-Yagüe, T. López-Royo, M. Casarejos, J. L. Lanciego, and I. Lastres-Becker, 'Cx3cr1-deficiency exacerbates alpha-synuclein-A53T induced neuroinflammation and neurodegeneration in a mouse model of Parkinson's disease.', *Glia*, vol. 66, no. 8, pp. 1752–1762, Aug. 2018, doi: 10.1002/glia.23338.
63. K. Biber, H. Neumann, K. Inoue, and H. W. G. M. Boddeke, 'Neuronal "On" and "Off" signals control microglia', Nov. 2007. doi: 10.1016/j.tins.2007.08.007.
64. J. F. Bazan *et al.*, 'A new class of membrane-bound chemokine with a CX3C motif.', *Nature*, vol. 385, no. 6617, pp. 640–4, Feb. 1997, doi: 10.1038/385640a0.
65. H. Li *et al.*, 'PGRN exerts inflammatory effects via SIRT1-NF- $\kappa$ B in adipose insulin resistance.', *J Mol Endocrinol*, vol. 64, no. 3, pp. 181–193, Apr. 2020, doi: 10.1530/JME-19-0211.
66. F. Negoita, J. Säll, B. Morén, K. Stenkula, and O. Göransson, 'Salt-inducible kinase 2 regulates TFEB and is required for autophagic flux in adipocytes.', *Biochem Biophys Res Commun*, vol. 508, no. 3, pp. 775–779, Jan. 2019, doi: 10.1016/j.bbrc.2018.11.177.
67. H.-H. Wang *et al.*, 'Activation of salt-inducible kinase 2 promotes the viability of peritoneal mesothelial cells exposed to stress of peritoneal dialysis', *Cell Death Dis*, vol. 7, no. 7, pp. e2298–e2298, Jul. 2016, doi: 10.1038/cddis.2016.79.

**Disclaimer/Publisher's Note:** The statements, opinions and data contained in all publications are solely those of the individual author(s) and contributor(s) and not of MDPI and/or the editor(s). MDPI and/or the editor(s) disclaim responsibility for any injury to people or property resulting from any ideas, methods, instructions or products referred to in the content.